Properties of the $\mathrm{a}_0(980)$ Meson

S. Teige, B. B. Brabson, R. R. Crittenden, A. R. Dzierba, J. Gunter, R. Lindenbusch, D. R. Rust, E. Scott, P. T. Smith, and T. Sulanke
Department of Physics, Indiana University,Bloomington IN 47405, USA

S. U. Chung, R. W. Hackenburg, C. Olchanski, S. Strassburger, D. P. Weygand, and H. J. Willutzki
Department of Physics, Brookhaven National Laboratory,Upton, L.I., NY 11973

Z. Bar-Yam, J. P. Cummings, J. P. Dowd, P. Eugenio, M. Hayek, W. Kern, E. King, and N. Shenhav
Department of Physics, University of Massachusetts Dartmouth,North Dartmouth MA 02747,USA

V. A. Bodyagin, O. L. Kodolova, V. L. Korotkikh, M. A. Kostin, A. I. Ostrovidov, L. I. Sarycheva, N. B. Sinev, I. N. Vardanyan, and A. A. Yershov
Institute for Nuclear Physics, Moscow State University,Moscow, Russian Federation

D. S. Brown, T. K. Pedlar, K. K. Seth, J. Wise, and D. Zhao,
Department of Physics, Northwestern University,Evanston IL 60208, USA

T. Adams, J. M. Bishop, N. M. Cason, E. I. Ivanov, J. M. LoSecco, J. J. Manak, A. H. Sanjari, W. D. Shephard, D. L. Stienike, S. A. Taegar, and D. R. Thompson
Department of Physics, University of Notre Dame, Notre Dame IN 46556, USA

S.P.Denisov, V. Dorofeev, I.Kachaev, V.V.Lipaev, A.V.Popov and D.I.Ryabchikov
Institute for High Energy Physics,Protovino, Russian Federation

G. S. Adams, J. Kuhn, J. Napolitano, M. Nozar, J. A. Smith, D. B. White, and M. Witkowski
Department of Physics, Rensselaer Polytechnic Institute, Troy NY 12180,USA

(September 12, 1997)

Events of the type $\pi^- \mathrm{p} \to \mathrm{n}\eta\pi^+\pi^-$ and $\pi^- \mathrm{p} \to \mathrm{n}\eta\pi^0$ at 18 GeV/c are analyzed. The mass and width of the neutral and charged $\mathrm{a}_0(980)$ were determined. The neutral a_0 is found to have a mass of 0.991 ± 0.0025 GeV/c^2 and a width of 0.069 ± 0.011 GeV/c^2. A partial wave analysis technique yields 0.9983 ± 0.0040 and 0.072 ± 0.010 GeV/c^2 for the mass and width of the charged a_0.

This paper presents the results of an analysis to determine the parameters of charged and neutral $\mathrm{a}_0(980)$ mesons from the reactions $\pi^- \mathrm{p} \to \eta\pi^+\pi^-\mathrm{n}$ and $\pi^- \mathrm{p} \to \eta\pi^0\mathrm{n}$ at 18.3 GeV/c. The data were taken during the 1994 running period of the Brookhaven National Laboratory (BNL) alternating gradient synchrotron (AGS) by the E852 collaboration.

The next section gives a description of the experiment and apparatus. The E852 apparatus included significant upgrades to the multiparticle spectrometer facility (MPS): the addition of a Lead Glass Detector (LGD) for photon detection, a large downstream drift chamber, target region instrumentation, an upgraded data acquisition system (DAQ), and a new trigger system.

The third section presents the results of the analysis of our data. The main points of this section include determination of the parameters of the $\mathrm{a}_0(980)$ (formerly the δ). The low values of the mass and width have been problematic when attempting to assign this state to the $^3P_0$ $q\overline{q}$ nonet. Some recent interpretations of this state are that it is a $qq\overline{qq}$ system [1], a hybrid meson [2], a $\mathrm{K}\overline{\mathrm{K}}$ molecule [3], a dynamically generated threshold effect [4], and, of course, as an ordinary $q\overline{q}$ meson. To further complicate matters, a possible replacement for the $a_0(980)$ in the filled scalar nonet has recently been reported [5].

Any interpretation of a particle must be consistent with measured properties of that particle. Several older experiments using $a_0(980)$ from $f_1(1285)$ decays [6,7] give a width near 0.06 GeV/c^2 and the highest statistics recent experiments give $\Gamma = 0.095 \pm 0.014$ GeV/c^2 for the charged $a_0(980)$ (1040 events) [8] and $\Gamma = 0.05412 \pm 0.00034 \pm 0.00012$ GeV/c^2 for the neutral $a_0(980)$ [9]. (The number of events observed by this experiment was not reported.) In this paper we report on the parameters of the charged $a_0(980)$ obtained from $f_1(1285)/\eta(1295)$ decay ($\approx$ 1400 events) and from directly produced neutral $a_0(980)$ ($\approx$ 720 events). The widths determined to date for the neutral and charged $a_0(980)$ are dramatically different. This experiment is the first to determine the parameters of the neutral and charged $a_0(980)$ from the same experiment.

The plan of the third section is as follows: we first present effective mass distributions showing evidence for our signals, we describe our analysis and reconstruction methods and determine the parameters of the charged $a_0(980)$. These parameters are found by two methods, a simple peak fitting technique and a method involving the variation of the $a_0(980)$ parameters in a partial wave analysis (PWA). We then present effective mass distributions from the two-body neutral final state reaction $\pi^- p \to \eta\pi^0 n \to 4\gamma n$, and redetermine the parameters of the neutral $a_0(980)$.

I. THE EXPERIMENT

The E852 apparatus (Fig. 1) consisted of a fully instrumented beamline, a hydrogen target, a recoil particle spectrometer, forward charged particle tracking, a large, segmented lead glass calorimeter and a nearly hermetic photon veto system. A flexible, programmable trigger allowed multiple final-state topologies to be collected simultaneously.

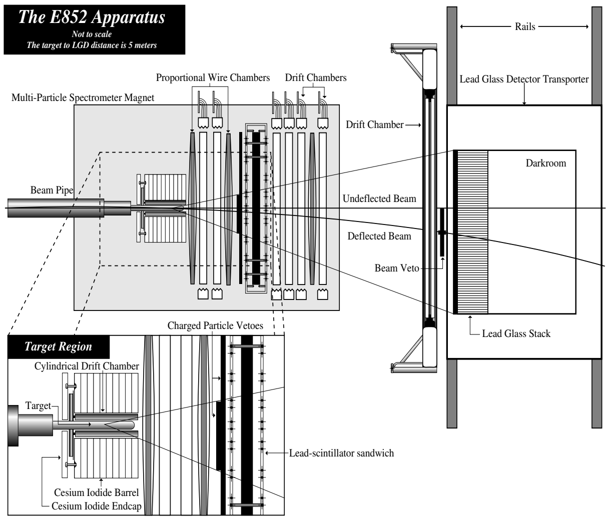

FIG. 1. An plan view of the experimental setup. The inset shows the target region, described in detail in the text. Proceeding downstream from the target the devices contained in the MPS magnetic field are a proportional wire chamber (PWC), two multiplane drift chambers, another PWC, a lead scintillator sandwich photon veto counter (DEA), three drift chambers, a PWC and a drift chamber. Further downstream and outside the MPS magnetic field are a large drift chamber and the lead glass detector (LGD).

The BNL high energy unseparated beam line (HEUB) delivered a beam of negatively charged particles to the MPS. Beamline instrumentation provided momentum and position analysis, particle identification, and beam definition for triggering. The maximum flux used by E852 was $\approx 2 \cdot 10^6$ particles/sec. At 18.3 GeV/c the momentum bite, $\Delta p/p$, was 3% and the π^- fraction of the beam approximately 99 %.

There were six tracking stations along HEUB. Each tracking station consisted of proportional wire chambers (PWCs) and scintillator hodoscopes. There were two tracking stations upstream of momentum analyzing dipoles and two stations immediately downstream to provide a momentum measurement with a resolution, $\delta p/p$, of less than 1 % . An additional two stations were placed immediately after a focusing quadrupole triplet to allow extrapolation of the beam track to the target.

There were three Čerenkov counters in the beam line. The first was a high pressure counter filled with with freon used for K/π separation. The rest were air-filled and were used for e/π separation.

E852 used a 12-in. liquid hydrogen target with a diameter of approximately 2.5 in. The target vessel was constructed of aluminum with $\approx$ 1 mil mylar windows on the upstream and downstream ends. The hydrogen content corresponded to 3% of an interaction length.

The region surrounding the liquid hydrogen target was upgraded for E852 by the addition of a cylindrical drift chamber (TCYL) and a cesium iodide barrel (CsI). These detectors were used to determine the identity of the recoil particle. Identification of the recoil particle as a neutron or proton is required for analysis of exclusive final states.

To identify low momentum recoil protons, a cylindrical drift chamber, TCYL, surrounded the target. TCYL was instrumented to perform as both a trigger element and as position measuring device. The number of wires struck in each event was available to the trigger logic and the signal from each wire was also digitized to allow a position measurement. Charge division was used to obtain the longitudinal position and a resolution of 7 mm was achieved. The azimuthal resolution was 0.4 mm. Details of the chamber design, construction, and instrumentation can be found in [10].

Surrounding the target and TCYL was a segmented soft photon veto constructed of thallium-doped cesium iodide crystals, denoted CsI. The CsI detector served to tag events in which a Δ, N^* or Λ was produced. It also served to tag soft photons in the final state that would otherwise miss the LGD.

The CsI detector consisted of a barrel and an upstream ring, designated CIB and CIR. CIB consisted of 10 rings of 18 crystals, each 5.0 cm long (z-length) and 7.5 cm thick (radial length). CIR consisted of a single ring of 18 crystals, each 7.5 cm long and 12.8 cm thick. The radiation length of the cesium iodide is 1.85 cm. A Hamamatsu 3590-01 photodiode was mounted on each block. Details of this detector's performance characteristics and design can be found in [11].

Charged particle reconstruction was achieved with a magnetic spectrometer. The MPS magnet was a large, 'C' shaped dipole magnet 450 cm long, with a vertical aperture of 130 cm and a horizontal aperture of 280 cm providing a 1-Tesla field.

The primary E852 tracking components are six identical drift chambers, denoted DM1-DM6. The active regions of the chambers measured 102 cm in y (the magnetic field direction was along $-\hat{y}$) and 174 cm in x (towards the top of Fig. 1). Each chamber consisted of seven planes: three x planes, two y planes, one u plane, and one v plane (The u and v planes are rotated $\pm 30^\circ$ with respect to the x planes). One x and one y plane in each chamber is offset by 1/2 the wire spacing in order to resolve the ambiguities associated with drift chambers. The readout electronics were custom built at BNL, and consisted of a 256-bit shift-register TDC for each channel. The full drift-distance spanned 16 TDC bins, each bin 4 ns in width. Digitization was performed in FASTBUS modules (also built at BNL) which encoded the data into a buffer for readout by the DAQ system. Drift chamber spatial resolution was $400\ \mu m$. The chamber construction and electronics design is fully documented elsewhere [12] - [16].

Proportional wire chambers (PWCs) were used for triggering and tracking. These chambers were of identical construction, each chamber consisting of 672 wires spaced 0.1 in. apart. The first two chambers are used for triggering as well as offline track reconstruction. The number of hits contained in the central regions of these chambers was available to the trigger system via custom electronics. The most downstream chamber was not included in the trigger but was used for track reconstruction.

The drift chamber farthest downstream, denoted TDX4, was used to detect charged particles near the face of the LGD. Without TDX4 the standard MPS tracking system would be inadequate to determine positions of charged tracks at the face of the LGD with sufficient accuracy to reject showers in the LGD associated with hadronic interactions. TDX4 does not contribute significantly to the momentum resolution of the charged tracks, due to its placement in the relatively small fringe field of the magnet. The sensitive area of TDX4 measured 305 cm x 200 cm, and consisted of five planes: three planes of cathode wires with a 0.4 cm pitch and two planes of alternating sense and field wires with a 0.8 cm pitch. The planes were separated by 1.6 cm. A spatial resolution of 150 μm was achieved.

The Downstream Endcap Array (DEA) was a lead/scintillator sandwich designed to detect photons that would miss the LGD and consisted of 4 sections forming a “picture frame” arrangement. Each section consisted of 18 layers of lead and 18 layers of scintillator. The first 12 layers of lead were 0.073 in. thick (1/3 radiation length) and the next 6 layers were each 0.146 in thick (2/3 radiation lengths). Each layer of scintillator is 0.196 in. thick. The thickness of the entire detector corresponds to 8.21 radiation lengths.

To avoid vetoing events in which only a charged track struck the DEA, a large scintillation detector (CPVC) that mirrored the geometry of the DEA was placed directly upstream of the DEA. A coincidence could be formed between these detectors, with a photon hit corresponding to $\overline{CPVC} \cdot DEA$. In addition, a charged particle veto (CPVB) was placed in the aperture of DEA to aid in the veto efficiency for non-interacting beam tracks for an all neutral trigger. Both CPVB and CPVC were 5mm thick.

The first level trigger for the experiment required an interaction in the target. At 18 GeV, the elastic scattering cross-section accounts for 4 mb [17] of the total $\pi^- p$ cross section of 25 mb. [18,19] It was desirable, therefore, to veto as much of the elastic cross section as possible. This was accomplished by exploiting the fact that the elastic cross-section is very strongly peaked in the forward direction ($d\sigma/dt \approx \exp(9t)$ [17]).

Two counters, the beam veto (BV) and the elastic veto (EV), were installed between the LGD and TDX4. The BV consists of a 4×6 in. piece of 1/4 in. thick scintillator. EV was a larger, circular counter, 12 in. in diameter. BV was positioned in the center of EV. The combined EV/BV system vetoed 89% of elastic scattering events.

The Lead Glass Detector (LGD) consisted of an array of 3045 4 cm × 4 cm × 45 cm type F8-00 lead glass blocks with a radiation length of 3.17 cm stacked in a 43 block × 71 block rectangle (four corner blocks were removed for ventilation purposes and four central blocks were removed to allow passage of the beam). The blocks were wrapped in 1 mil. aluminized mylar for optical isolation. Čerenkov light produced by interacting photons and electrons was measured by type FEU-84-3 Russian-built photomultipliers. High voltage for the photomultipliers was supplied by computer-controlled Cockcroft-Walton type bases. The tube/base assemblies were held in an aluminum and soft iron structure. The entire assembly was carried by a transporter to allow each module to be placed in an electron beam for calibration. A laser-based monitoring system was used to illuminate the detector to monitor fluctuations in phototube gains. The glass, photomultipliers and bases are described in detail in Reference [20,21].

The calibration of the LGD was monitored by a laser based monitoring system. A pulsed nitrogen laser excited a small cylinder of scintillator inside the laser enclosure. The scintillator illuminated a bundle of optical fibers, 18 of which carried light to the edges of three 39 in. × 69 in × 0.5 in. acrylic sheets mounted directly in front of the wall of lead glass blocks. Sufficient light was scattered out of the acrylic sheets and onto the photocathodes to give a pulse with an amplitude equivalent to a 7 GeV shower, approximately 1000 ADC counts. An additional four fibers carried light to an RCA 8575 photomultiplier tube in the darkroom at the same (controlled) temperature as the photomultipliers of the lead-glass wall. In addition, this control tube was magnetically shielded. The signals from this tube were used to measure the pulse to pulse variation of the laser output.

One of the important design features of E852 was the ability to trigger on multiple final state topologies simultaneously. In order to accomplish this goal, a robust programmable trigger system was constructed. The trigger was broken up into three stages, pretrigger, Level 1 and Level 2. The pretrigger (an interaction requirement) produced gates for various detector components and the Level 1 trigger (charged particle multiplicity and photon vetos) selected events with specific charged particle multiplicities and good photon containment. The Level 2 trigger selected events using energy and effective mass information from the LGD.

The pretrigger was defined as a pattern of hits in the beamline scintillators consistent with the passage of a single charged particle in coincidence with no hit in the EV or BV. This fast trigger component selected interacting pions.

The Level 1 trigger combined the trigger information from all remaining detector components except the LGD trigger processor, that is, the DEA, CPVB, CPVC, TCYL and the first two PWCs. Logical functions of these trigger elements were evaluated using memory look up units. These logical functions selected the charged particle topology of the events. Several triggers were implemented corresponding to zero, one, two, three or four charged tracks going forward.

The zero-track topology required that there be no signals in DEA, CPVB, CPVC, TCYL or the first two PWCs. Triggers with an odd number of forward tracks required the correct number of hits in the first two PWCs and at least one hit in each cylinder of TCYL (from the recoiling charged particle required by charge conservation). Because the forward going tracks from even multiplicity events could strike the inner cylinders of TCYL, the TCYL requirement was relaxed for these topologies to require only the absence of hits in the outermost cylinder. The naming convention for these triggers is (number of TCYL tracks)-(number of TPX1 hits) -(number of TPX2 hits). For example, for events with two charged particles in the final state and a neutron recoil the trigger is denoted 0-2-2. No requirement on the state of the CsI was imposed.

An important feature of the trigger in experiment E852 was the ability to calculate the effective mass and total energy of the photon system detected in the LGD. To accomplish this, the neutral energy deposited in the LGD was read out, digitized by fast ADCs, and processed by a fast trigger processor in a total time of approximately 10 μs. The trigger processor was able to handle up to 10^4 events per second at 10% dead time. Details of the trigger processor can be found in [21].

The final experimental triggers from the Level 2 trigger were:

- 0-0-0 $\cdot$TriggerProcessor$_{\mathrm{energy}}$
- 1-1-1 $\cdot$TriggerProcessor$_{\mathrm{eta}}$
- 0-2-2 $\cdot$TriggerProcessor$_{\mathrm{eta}}$
- 1-3-3 $\cdot$TriggerProcessor$_{\mathrm{eta}}$
- 1-3-3

where TriggerProcessor$_{\mathrm{energy}}$ denotes the requirement that the LGD contained energy consistent with the beam energy and TriggerProcessor$_{\mathrm{eta}}$ denotes the requirement that the trigger processor detected an effective mass in the LGD greater than the mass of the pion.

II. ANALYSIS

Data for this analysis were collected using the zero and two forward-going charged track topology triggers which we denote as 0-0-0 and 0-2-2 respectively. In both samples we demand a reconstructed $\eta \to 2\gamma$ decay. We also assume that the forward going charged particles on the 0-2-2 system are pions.

The $\eta\pi$ system is analyzed for the $\mathrm{a}_0^\pm$ and a_0^0 parameters using the full power of the experiment, including our sensitivity to different channels and PWA techniques. Although we clearly observe the a_0^0 directly through $\pi^-\mathrm{p} \to \mathrm{a}_0^0\mathrm{n}$ and use this to derive its parameters, we observe at best a very weak signal of a_0^- in $\pi^-\mathrm{p} \to \mathrm{a}_0^-\mathrm{p}$. We therefore determine the $\mathrm{a}_0^\pm$ parameters in the reaction $\pi^-\mathrm{p} \to \eta\pi^+\pi^-\mathrm{n}$ with $M_{\eta\pi\pi}$ near the $\mathrm{f}_1(1285)/\eta(1295)$.

The analyses of the different charge states of the a_0 are discussed in the following two subsections.

A. The Charged a_0

Events with two reconstructed, forward going tracks (assumed to be pions) are considered first. Fig. 2 shows the observed $\eta\pi^+\pi^-$ effective mass distribution. Events in this plot were selected by requiring that there were exactly two reconstructed charged tracks, exactly two photon clusters in the lead glass detector, and that the effective mass of the photon pair be between 0.5 and 0.6 GeV/c^2 . The photon energies were fitted using the η and neutron masses as constraints and the fitted values were used for the evaluation of the effective masses presented below.

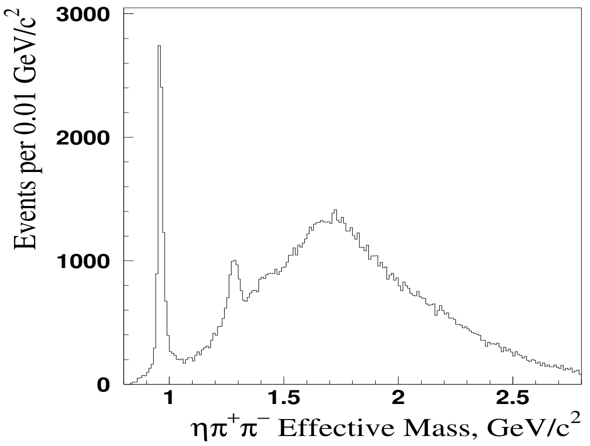

FIG. 2. The observed $\eta\pi^+\pi^-$ effective mass distribution.

Clear structure associated with the $\eta'(958)$ and near 1.28 GeV/c^2 is seen. The η' seen in this decay mode and in $\eta' \to \eta\pi^0\pi^0 \to 6\gamma$ has been used to verify the mass scale of the experiment. The results for the mass of the η' as determined from these two modes are consistent with each other and, with the world average, within 0.001 GeV/c^2 .

There are two known states decaying into $\eta\pi\pi$ near 1.28 GeV/c^2 and we will refer to this structure as $f_1(1285)/\eta(1295)$ in the following. Additionally, a shoulder near 1.4 GeV/c^2 can be seen. We defer comment on the nature of this structure until a complete partial wave analysis (currently underway) is completed.

Fig.3 shows the $\pi^+\pi^-$ and $\eta\pi^\pm$ effective mass distributions. Structures associated with the $\rho(770)$, $a_0(980)$ and $a_2(1320)$ are clearly visible. The structures near threshold in these plots are due to the large number of $\eta' \to \eta\pi^+\pi^-$ events present in this data sample.

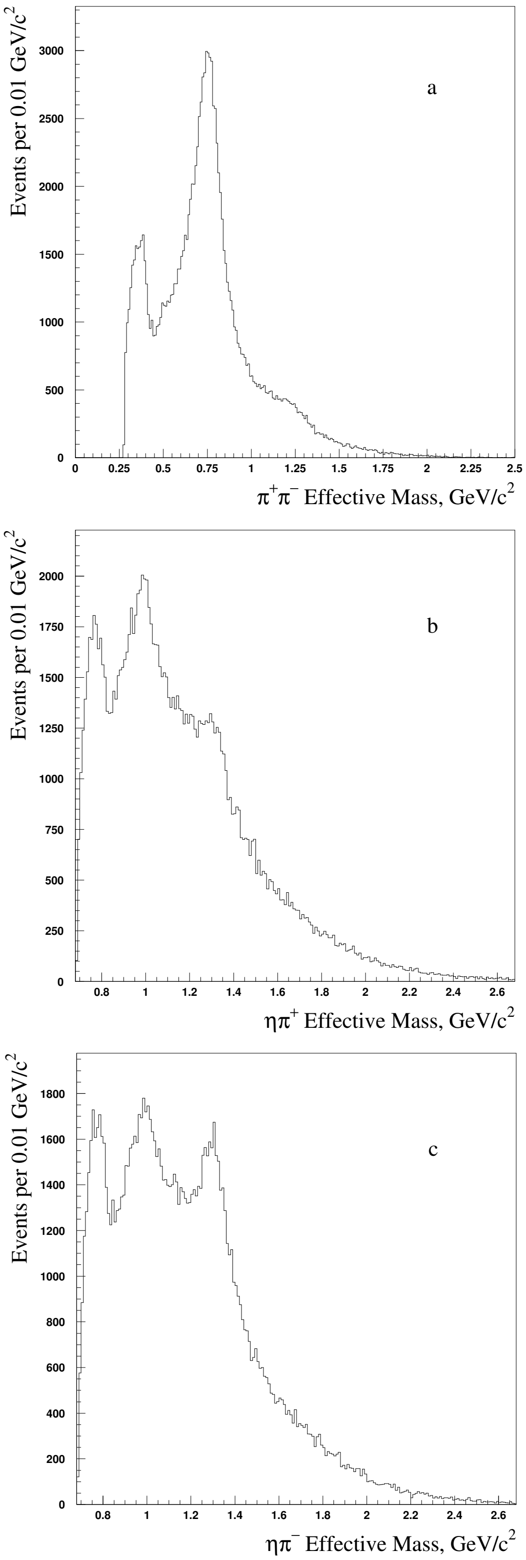

FIG. 3. The $\pi^+\pi^-$ (a), $\eta\pi^+$ (b) and $\eta\pi^-$ (c) effective mass distributions. The $\rho(770)$ is clearly visible in (a) and the $a_0(980)$ and $a_2(1320)$ are evident in (b) and (c). No acceptance correction has been made.

Fig. 4 shows the Dalitz plot and its projections for events with an $\eta\pi\pi$ mass near 1.28 GeV/c^2 . A clear a_0^+ band is seen but there is scant evidence for an a_0^- band. Monte-Carlo calculation has shown that this is not an effect of the finite acceptance of the apparatus. A PWA (discussed below) indicates this effect is due to interference between an isospin one $\rho\eta$ state and the isospin zero $f_1(1285)/\eta(1295)$ states. These effects show that caution must be excercised when fitting projections of the Dalitz plot.

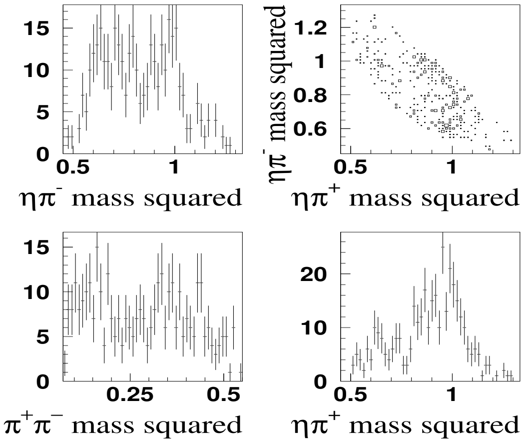

FIG. 4. A typical Dalitz plot and its projections. The projections are from threshold to the maximum kinematically allowable value of the effective mass squared in 50 bins. The units are (GeV/c^2)^2. The range of $\eta\pi^+\pi^-$ effective mass used to fill the plots was (1.28 - 1.29) GeV/c^2.

A PWA is used to extract the $a_0^\pm$ mass and width using a Breit-Wigner parameterization. The PWA is also used to establish cuts which enhance the $a_0^\pm$ signal in such a way that a simple "peak+background" fit yields consistent results. We use this data sample for a fit with the parameterization of Flatté. [22] The PWA method used to determine the Breit-Wigner parameters of the $a_0^\pm$ is described below.

Multiple partial wave fits were performed on the $\eta\pi^+\pi^-$ data set in the $f_1(1285)/\eta(1295)$ region. For each fit, the mass and width of the a_0 was varied until a minimum in the negative log likelihood function was found. The $\eta\pi^+\pi^-$ system was described as a superposition of states characterized by spin, parity, and C-parity (J^{PC}), the absolute value of projection of spin on the quantization axis (m), the isobar of the decay, the orbital angular momentum between the isobar and the bachelor (l), and the reflectivity (ϵ), which is defined to correspond to the naturality of the exchanged particle. We have applied the parametrization of Chung and Trueman [23], which ensures that the conditions of positivity and parity conservation in the production process are satisfied with the minimum number of parameters. The method used is described in detail elsewhere [24] and some explicit formulae are given in the appendix.

The intensity distribution is described by:

$$I(\tau) = \sum_{\epsilon\nu\nu'} {}^{\epsilon}\rho_{\nu\nu'}\, {}^{\epsilon}A_{\nu}(\tau)\, {}^{\epsilon}A^{*}_{\nu'}(\tau) \qquad (2.1)$$

where

$$\nu = J^{PC} lm\{isobar\}\{bachelor\} \qquad (2.2)$$

${}^{\epsilon}A_{\nu}$ is the amplitude for the decay of the $\eta\pi^{+}\pi^{-}$ system and the subsequent decay of the isobar. The spin-density matrix is given by:

$${}^{\epsilon}\rho_{\nu\nu'} = \sum_{k} {}^{\epsilon}V_{\nu k}\, {}^{\epsilon}V^{*}_{\nu' k} \qquad (2.3)$$

where ${}^{\epsilon}V_{\nu k}$ are complex parameters obtained in the fit and are proportional to the production amplitudes. The index k refers to the two sets of mutually non-interfering amplitudes corresponding to nucleon spin flip and non-flip used in this analysis.

Each fit was performed on 1318 $\eta\pi^{+}\pi^{-}$n events in the $\eta\pi^{+}\pi^{-}$ mass region between 1.265-1.305 GeV . All fits used the set of waves shown in Table I, with the addition of an incoherent background wave. Fits with different values of the mass and width of the $a_0(980)$ isobar were made, and the negative log likelihood function was obtained for each fit. The results of these fits as a function of the parameters of the $a_0(980)$ are shown in Fig. 5. Using this method the mass and the width of the a_0 were determined to be (0.9983 ± 0.0040) and (0.072 ± 0.010) GeV/c^2 , respectively. A change in the log likelihood function of 1/2 was used to determine the quoted errors. A correction for the width, discussed below, has been applied.

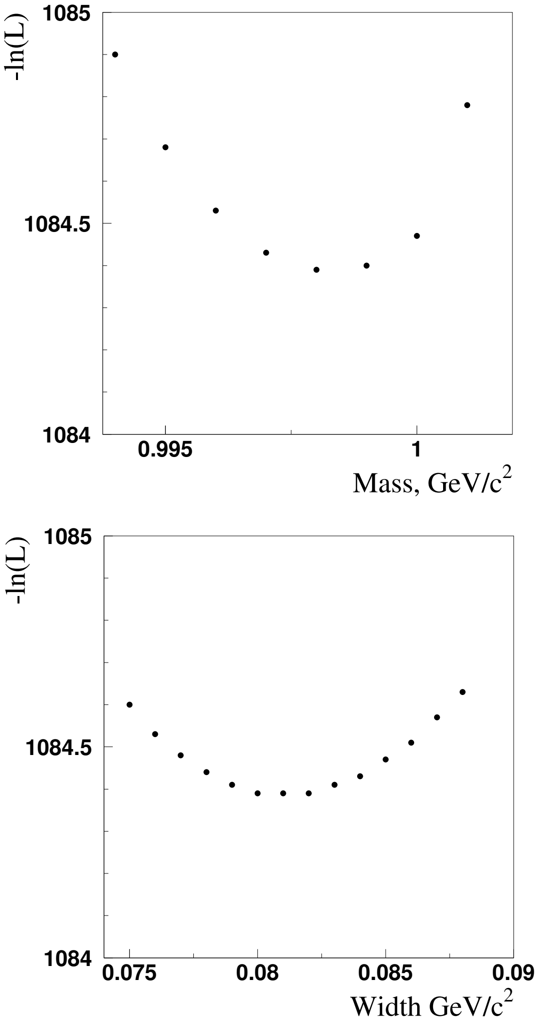

FIG. 5. The results partial wave analysis fits. Shown is $-\ln(\mathcal{L})$ as a function of the mass (top) and width of the $a_0(980)$ used in the fits.

J^{PC}	*isobar/bachelor*	l	m	ϵ
1^{--}	ρ/η	P	0	-
1^{+-}	ρ/η	S	0	+
0^{-+}	a_0/π	S	0	+
1^{++}	a_0/π	P	0	+
0^{-+}	σ/η	S	0	+

TABLE I. Partial Waves used in the fit

Because the above analysis determined that the $f_1(1285)/\eta(1295)$ has a decay into $\eta\pi\pi$ via $a_0\pi$ this fact can be exploited to select a set of events with an enhanced population of $a_0 \to \eta\pi$ decays. To take into account interference effects a Monte-Carlo data set with I=0 and I=1 interference was studied. It was found that eliminating events with $M_{\pi\pi} \geq 0.65$ GeV/c^2 (near the mass of the ρ) and events with $\mid M_{\eta\pi^-} - 0.99 \mid \leq 0.040$ GeV/c^2 (near the mass of the a_0^-) allowed the recovery of the a_0 parameters used to generate the Monte-Carlo sample.

The $\eta\pi^+$ effective mass distribution, subject to the requirements above and the additional requirement that the $\eta\pi\pi$ mass be within $\pm$ 0.020 GeV/c^2 of 1.29 GeV/c^2, is shown as Fig. 6. The mass and width of the a_0^+ are determined to be 0.9964 ± 0.0016 and 0.062 ± 0.006 GeV/c^2 respectively. A relativistic, S-wave Breit-Wigner form was used to extract these parameters. The two determinations of the mass and width are statistically consistent.

The width has been corrected for detector resolution by a Monte-Carlo calculation that reproduces the observed width (0.0251 GeV/c^2) of the $\gamma\gamma$ system from the η decay. Monte-Carlo data sets were generated with varying input values for width of the $a_0(980)$. These data sets were subjected to the same fitting procedures used for the experimental data. The quoted width is the Monte-Carlo input value that reproduced the observed width of the fit to the data.

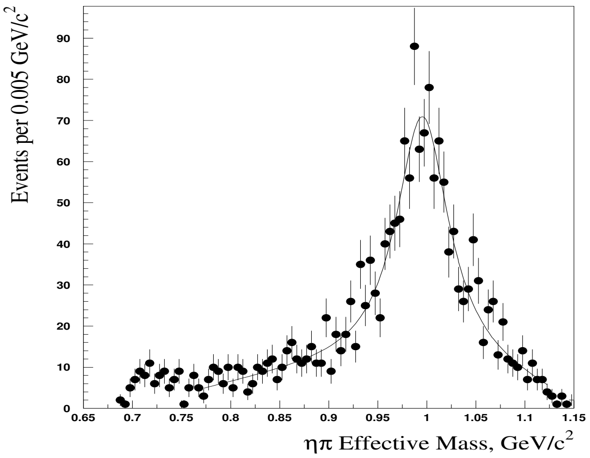

FIG. 6. The observed $\eta\pi^+$ effective mass distribution and a fit to a Breit-Wigner plus third order polynomial. The χ^2 per degree of freedom was 1.24.

Another parameterization, due to Flatté, [22] of the shape of the $a_0(980)$ based on a coupled channel $(\eta\pi, K\overline{K})$ description is available. Briefly,

$$\frac{d\sigma}{dM} = C \mid A \mid^2 \tag{2.4}$$

with

$$A = \frac{\sqrt{\Gamma_0 \Gamma_{\eta\pi}} \mathrm{M_r}}{\mathrm{M_r}^2 - \mathrm{M}^2 - i\mathrm{M_r}(\Gamma_{\eta\pi} + \Gamma_{\overline{K}K})}, \tag{2.5}$$

$$\Gamma_{\eta\pi} = \mathrm{g}_{\eta\pi} q \tag{2.6}$$

and

$$\Gamma_{\overline{K}K} = i\mathrm{g}_{\overline{\mathrm{K}}\mathrm{K}} \sqrt{\mathrm{M_K}^2 - (\mathrm{M}/2)^2} \tag{2.7}$$

below $\overline{K}K$ threshold and

$$\Gamma_{\overline{K}K} = \mathrm{g}_{\overline{\mathrm{K}}\mathrm{K}} \sqrt{(\mathrm{M}/2)^2 - \mathrm{M_K}^2} \tag{2.8}$$

above threshold. q is the momentum of the η in the rest frame of the $\mathrm{a_0}(980)$, $\mathrm{g}_{\overline{\mathrm{K}}\mathrm{K}}$ and $\mathrm{g}_{\eta\pi}$ are coupling constants to the two final states, $\mathrm{M_r}$ is the mass of the $\mathrm{a_0}(980)$ and $\mathrm{M_K}$ is the mass of the kaon. Following Flatté, the parameter Γ_0 is set to $\mathrm{g}_{\eta\pi} q$ evaluated at $\mathrm{M} = \mathrm{M_r}$. We choose $\mathrm{g}_{\eta\pi}$ and

$$\mathrm{R} = \frac{\mathrm{g}_{\overline{\mathrm{K}}\mathrm{K}}}{\mathrm{g}_{\eta\pi}} \tag{2.9}$$

as our fit parameters. The best fit of our data obtained with this parameterization is shown in Fig. 7.

The parameters found were $\mathrm{M_r} = 1.001 \pm 0.0019$ GeV/c^2 , $\mathrm{g}_{\eta\pi} = 0.243 \pm 0.015$ and $\mathrm{R} = 0.91 \pm 0.10$. These values can be compared to Bugg *et al.* [25] who obtain $\mathrm{R} = 1.16 \pm 0.18$ and $\mathrm{M_r} = 0.999 \pm 0.005$ GeV/c^2 . Given a value of $\mathrm{g}_{\eta\pi}$ and of $\mathrm{M_r}$ $\Gamma_{\eta\pi}$ can be evaluated at $\mathrm{M} = \mathrm{M_r}$. The value we obtain, after a resolution correction as discussed above, is $\Gamma = 0.070 \pm 0.005$ GeV/c^2 .

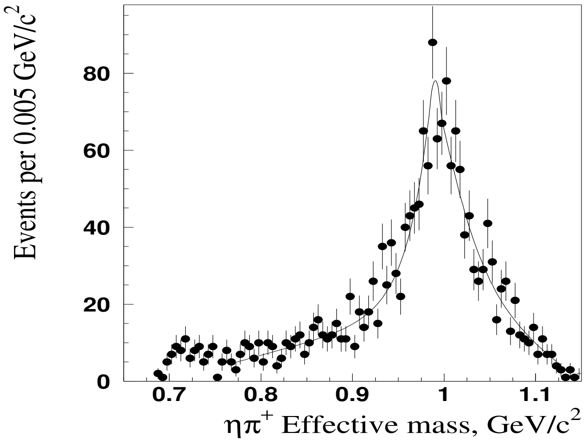

FIG. 7. The observed $\eta\pi^+$ effective mass distribution and a fit to the parameterization of Flatté plus third order polynomial. The χ^2 per degree of freedom was 1.17.

B. The Neutral a_0

In this experiment we also observe the neutral $a_0(980)$ in the decay $a_0(980) \to \eta\pi^0 \to 4\gamma$. A data sample was selected by requiring:

- There were no charged tracks in the event.
- Exactly four photons were reconstructed in the LGD.
- The total energy deposited in the LGD was consistent with a forward going system decaying entirely into photons. This selected events which were fully contained in the LGD active area.
- There were no clusters in the LGD within 2 cm of the edge of the beam hole. These events were eliminated because the energy and position of photons near the beam hole is poorly measured due to energy losses into the uninstrumented beam hole.
- The χ^2 probability for the best combination of photons under the $\pi^0\pi^0$ hypothesis was less than 3%.
- The χ^2 probability for the best combination of photons under the $\eta\pi^0$ hypothesis was greater than 15%.

A constrained fit using only the η and π^0 masses was performed to get an improved estimate of the photon energies. The photon momenta were calculated geometrically using the observed position of the photon cluster in the LGD and the center of the target to determine the photon direction. The resulting $\eta\pi^0$ effective mass distribution is shown as Fig. 8.

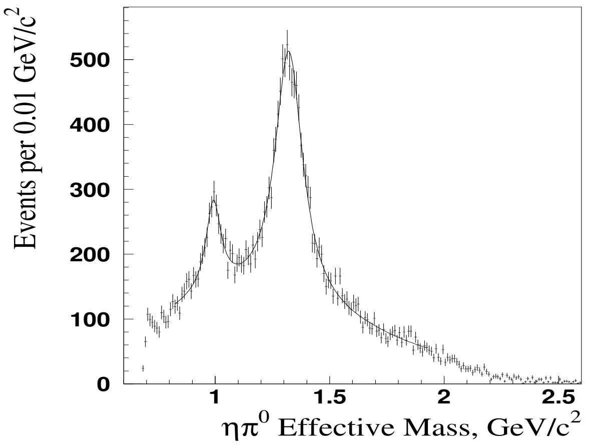

FIG. 8. The observed $\eta\pi^0$ effective mass distribution. The χ^2 per degree of freedom was 0.99 for 90 degrees of freedom. The smooth curve is a sum of two Breit-Wigner distributions plus a third order polynomial.

Clear structures associated with the $a_0(980)$ and $a_2(1320)$ are visible in Fig. 8. There are $\approx$ 720 $a_0(980)$ events and $\approx$ 4900 $a_2(1320)$ events. The distribution shown in Fig. 8 was fitted to the sum of two Breit-Wigner distributions and a third order polynomial over the region from the 0.8 to 1.8 GeV/c^2 . The result for the $a_0(980)$ was $M = 0.9910 \pm 0.0025$ and $\Gamma = 0.069 \pm 0.011$ GeV/c^2 . The width has been corrected for experimental resolution as described previously.

III. CONCLUSIONS

TABLE II. The parameters of the $a_0(980)$ with a comparison to previous results. The different analysis methods used for this experiment are referred to as A, a fit to the $a_0(980)$ parameters using a partial wave analysis B, a fit to an effective mass distribution and C, a fit to an effective mass distribution with the Flatté form

Charged a_0				
Mass (GeV/c^2)		Width (GeV/c^2)		Ref.
0.986	±0.003	0.062	±0.011	[6]
0.990	±0.007	0.060	±0.011	[7]
0.984	±0.004	0.095	±0.011	[8]
0.999	±0.005			[22]
0.976	±0.006			[25]
0.9983	±0.0040	0.072	±0.010	E852 (A)
0.9958	±0.0016	0.062	±0.006	E852 (B)
1.0013	±0.0019	0.070	±0.005	E852 (C)
Neutral a_0				
Mass (GeV/c^2)		Width (GeV/c^2)		Ref.
0.98445	±0.00123	0.05412	±0.00034	[9]
	±0.00034		±0.00012	
0.9910	±0.0025	0.069	±0.011	E852 (B)

The results of the fits discussed above are summarized in Table II and a comparison with previous results is given. Additionally, the Flatté parameters

$$g_{\eta\pi} = 0.24 \pm 0.015 \tag{3.1}$$

and

$$R = 0.91 \pm 0.10 \tag{3.2}$$

are determined. This experiment favors slightly higher values for the mass of the $a_0(980)$ than have been previously observed. This is found for both the neutral and charged $a_0(980)$. The neutral a_0 is found to have a width within 1.4 σ of the highest statistics previous measurement. The charged a_0 is found to have a width consistent with recent previous measurements. We estimate the charged-neutral mass difference to be 0.005 to 0.010 GeV/c^2 with the charged $a_0(980)$ being heavier than the neutral $a_0(980)$.

ACKNOWLEDGMENTS

We would like to express our deep appreciation to the members of the MPS group at BNL. Without their outstanding efforts, the results presented here could not have been obtained. We would also like to acknowledge the invaluable assistance of the staffs of the AGS and BNL, and of the various collaborating institutions. This research was supported in part by the National Science Foundation and the US Department of Energy.

APPENDIX A

The kinematics of the event

$$\pi^- p \rightarrow X n \tag{A1}$$

followed by

$$X \rightarrow \{isobar\}\{bachelor\} \tag{A2}$$

and

$$\{isobar\} \rightarrow ab \tag{A3}$$

is specified completely by the beam momentum, momentum transfer (t), mass of particle X, 4 angles and the effective mass of the (a, b) system.

The decay angles of $X \rightarrow \{isobar\}\{bachelor\}$ are denoted as (Θ, Φ) , $\{isobar\} \rightarrow ab$ as (θ, ϕ) and the effective mass of the (a, b) system as w. The angles (Θ, Φ) are the polar and azimuthal angles of the isobar momentum vector in the center of mass of the parent particle X (the Gottfried-Jackson frame). The momentum of the isobar in this frame is denoted as p below. The Gottfried-Jackson frame is oriented such that the z-axis is parallel to the beam momentum and the y-axis is along the production normal, defined to be the cross product of the beam momentum with the momentum of X in the center of mass of the (beam+target) system.

The angles (θ, ϕ) are the polar and azimuthal angles of the momentum vector of one of the decay products (a or b , denoted as q below) in the rest frame of the isobar. The z-axis of this frame is defined as parallel to the momentum vector of the isobar in the Gottfried-Jackson frame. The y-axis is parallel to the cross product of the Gottfried-Jackson frame z-axis with the isobar momentum evaluated in the Gottfried-Jackson frame.

To analyze an experiment in terms of a partial wave expansion it is necessary to write the decay amplitude for each partial wave needed to describe the data. This amplitude depends on all eight kinematic quantities defined above. In the following, we assume a constant beam momentum and that the analysis will be performed in a small “bin” of three body effective mass and momentum transfer.

The amplitude associated with a particular partial wave now depends only on five kinematic quantities. That is,

$$ {}^{\epsilon}A_{\nu}(\tau) = {}^{\epsilon}A_{\nu}(\Theta, \Phi, \theta, \phi, w) \tag{A4}$$

where the quantities ϵ and ν denote a set of quantum numbers and the choice of isobar used to define this particular partial wave.

This amplitude can be written as

$$ {}^{\epsilon}A_{\nu}(\Theta, \Phi, \theta, \phi, w) \propto \sqrt{(2s+1)}\Delta(m) f(w)\sqrt{2l+1} \times \\ \sum_{\lambda} (l0s\lambda|J\lambda)\left[D^{J*}_{m\lambda}(\Theta, \Phi, \phi) + \epsilon D^{J}_{m\lambda}(\Theta, \Phi, \phi)\right] d^{s*}_{\lambda 0}(\theta) \tag{A5}$$

where the bracketed sum of “D-functions” describes the angular dependence of the decay of X , the final d-function describes the decay of the isobar, given the decay of X and $f(w)$ contains all dependence of the amplitude on the mass of the isobar and the mass of the (a, b) system. J is the total spin of X and m its z-component. s is the total spin of the isobar and λ its helicity. l is the orbital angular momentum of the isobar-bachelor system. ϵ is the “reflectivity”, defined to equal the naturality of the exchange particle. $(l0s\lambda|J\lambda)$ is a Clebch-Gordon coefficient. The function Δ is given by

$$\begin{aligned} \Delta(m) &= \tfrac{1}{\sqrt{2}} \ \text{ if } m > 0 \\ &= \tfrac{1}{2} \ \text{ if } m = 0 \\ &= 0 \ \text{ if } m < 0 \end{aligned} \tag{A6}$$

The d-functions are given by

$$ d^{s}_{\lambda 0}(\theta) = \sqrt{\frac{4\pi}{2s+1}} Y^{\lambda}_{s}(\theta, \phi) e^{-i\lambda\phi}. \tag{A7}$$

Notice that the spherical harmonics, $Y^{\lambda}_{s}(\theta, \phi)$, contain a factor of $e^{i\lambda\phi}$ so that the d-functions do not depend on ϕ.

The D-functions are given by [27]

$$D^J_{m\lambda}(\Theta,\Phi,\phi) = \sqrt{\frac{(J-\lambda)!(J+m)!}{(J+\lambda)!(J-m)!}}\frac{(\cos\Theta/2)^{2J+\lambda-m}(-\sin\Theta/2)^{m-\lambda}}{(m-\lambda)!}e^{im\Phi}e^{i\lambda\phi}\times$$
$$ {}_2F_1(m-J,-\lambda-J,m-\lambda+1;-\tan^2\Theta/2) \quad \text{(A8)}$$

where ${}_2F_1(\alpha,\beta,\gamma;z)$ is the hypergeometric series. [28]

$$ {}_2F_1(\alpha,\beta,\gamma;z) = 1+\sum_{k=1}^{\infty}\frac{\alpha(\alpha+1)\cdots(\alpha+k-1)\beta(\beta+1)\cdots(\beta+k-1)}{k!\gamma(\gamma+1)\cdots(\gamma+k-1)}z^k. \quad \text{(A9)}$$

Notice that this series terminates for integer values of α or β.

The dependence of the amplitude on the mass of the (a,b) system is given by

$$f(w) = F_l(p)F_s(q)BW(w), \quad \text{(A10)}$$

$$BW(w) = \frac{w_0\Gamma_0}{w_0^2-w^2-iw_0\Gamma(w)}, \quad \text{(A11)}$$

$$\Gamma(w) = \Gamma_0\frac{w_0qF_s^2(q)}{wq_0F_s^2(q_0)}, \quad \text{(A12)}$$

w_0 and Γ_0 are the mass and width of the isobar, $q_0 = q(w_0)$ and $F_s(q)$ are the centrifugal-barrier factors as given by Hippel and Quigg. [29] For example,

$$F_0(q) = 1 \quad \text{(A13)}$$

$$F_1(q) = \sqrt{\frac{2z}{z+1}} \quad \text{(A14)}$$

with

$$z = \frac{q^2}{q_R^2}, \quad \text{(A15)}$$

We have taken q_R as 0.1973 GeV/c.

The total observed intensity is given by the square of a sum over the partial waves used in a particular analysis. Let ν be the set of quantum numbers of a particular partial wave, that is,

$$\nu = J^{PC}lm\{isobar\}\{bachelor\} \quad \text{(A16)}$$

The intensity distribution is then given by

$$I(\tau) = \sum_k\sum_{\epsilon\nu\nu'} {}^\epsilon V^\epsilon_{\nu k}V^*_{\nu' k}\,{}^\epsilon A_\nu(\tau)\,{}^\epsilon A^*_{\nu'}(\tau) \quad \text{(A17)}$$

where the summation extends over the partial waves considered and the ${}^\epsilon V_{\nu k}$ are to be determined by a fit to the data.

Defining

$$ {}^{\epsilon}\rho_{\nu\nu'} = \sum_k {}^{\epsilon}V_{\nu k}\, {}^{\epsilon}V^*_{\nu' k}. \tag{A18} $$

where index k extends over two non-interfering set of amplitudes corresponding to spin flip and spin non-flip at the neucleon vertex allows us to write

$$ I(\tau) = \sum_{\epsilon\nu\nu'} {}^{\epsilon}\rho_{\nu\nu'}\, {}^{\epsilon}A_{\nu}(\tau)\, {}^{\epsilon}A^*_{\nu'}(\tau). \tag{A19} $$

To determine the parameters ${}^{\epsilon}V_{\nu k}$ we use a maximum likelihood method. The likelihood of finding n events in a given bin is defined as a product of probabilities,

$$ \mathcal{L} \propto \left[\frac{\overline{n}^n}{n!} e^{-\overline{n}}\right] \prod_1^n \left[\frac{I(\tau_i)}{\int I(\tau)\eta(\tau)d\tau}\right] \tag{A20} $$

where $\eta(\tau)$ is the experimental acceptance. The quantity

$$ \overline{n} = \int I(\tau)\eta(\tau)d\tau \tag{A21} $$

is the number of events expected in the bin as predicted by the intensity function. The likelihood function can then be written as

$$ \mathcal{L} \propto \left[\prod_1^n I(\tau_i)\right] \exp\left[-\int I(\tau)\eta(\tau)d\tau\right] \tag{A22} $$

where terms that do not depend on the parameters of the fit have been dropped. The integral in eqn. A22 can be calculated by the Monte-Carlo method. We begin by inserting the expression for $I(\tau)$ into the integral

$$ \overline{n} = \int \eta(\tau) \sum_{\epsilon\nu\nu'} {}^{\epsilon}\rho_{\nu\nu'}\, {}^{\epsilon}A_{\nu}(\tau)\, {}^{\epsilon}A^*_{\nu'}(\tau) d\tau. \tag{A23} $$

Now, because the fitted parameters do not depend on the kinematic variables τ ,

$$ \overline{n} = \sum_{\epsilon\nu\nu'} {}^{\epsilon}\rho_{\nu\nu'} \int \eta(\tau)\, {}^{\epsilon}A_{\nu}(\tau)\, {}^{\epsilon}A^*_{\nu'}(\tau) d\tau \tag{A24} $$

and the order of the summation and integration can be exchanged. The final step is to approximate the acceptance as a sum over accepted Monte-Carlo events divided by the number of generated events. That is

$$ \int \eta(\tau)\, {}^{\epsilon}A_{\nu}(\tau)\, {}^{\epsilon}A^*_{\nu'}(\tau) d\tau \approx \frac{1}{M} \sum_i^{M_x} {}^{\epsilon}A_{\nu}(\tau_i)\, {}^{\epsilon}A^*_{\nu'}(\tau_i) \tag{A25} $$

where M is the total number of Monte-Carlo events generated, M_x is the total number of accepted Monte-Carlo events and the summation extends only over accepted events.

Defining the numerical factor

$$\eta_x = \frac{M_x}{M} \tag{A26}$$

and a function

$$\eta_x {}^{\epsilon}\Psi_{\nu\nu'}(\tau) = \frac{1}{M}\sum_i^{M_x} {}^{\epsilon}A_{\nu}(\tau_i)\, {}^{\epsilon}A^*_{\nu'}(\tau_i) \tag{A27}$$

allows us to write the log-likelihood function in the more compact form

$$\ln \mathcal{L} = \sum_i^n \ln(I(\tau)) - \eta_x \sum_{\epsilon\nu\nu'} {}^{\epsilon}\rho_{\nu\nu'} {}^{\epsilon}\Psi_{\nu\nu'}(\tau_i). \tag{A28}$$

[1] I.F. Iskhakov, Sov. Phys. J. **34** 578 (1991).
[2] S. Ishida *et al.*, 6th International Conference on Hadron Spectroscopy, Manchester, UK, Jul 10 - 14, 1995.
[3] Nathan Isgur, Kim Maltman, John Weinstein and Ted Barnes, Phys. Rev. Lett. **64** 161 (1990).
[4] G. Tanssen, B.C.Pearce, K. Holinde and J. Speth, Phys. Rev. **D52** 2690 (1995).
[5] C. Amsler *et al.*, Phys. Lett. **B333** 277 (1994).
[6] C. Evangelista *et al.*, Nucl. Phys. **B178** 197 (1981).
[7] A. Gurtu *et al.*, Nucl. Phys. **B151** 181 (1979).
[8] T. Armstrong *et al.*, Zeit. fur Phyz. **C52** 389 (1991).
[9] C. Amsler *et al.*, Phys. Lett. **B327** 425 (1994).
[10] Z. Bar-Yam et al., Nucl. Instrum. Meth. **A386** 235 (1997)
[11] T. Adams *et al.*, Nucl. Instrum. Meth. **A368** 617 (1996).
[12] E. Platner, IEEE Transactions on Nuclear Science. **NS-25, No. 1** 35 (1978).
[13] A. Etkin, IEEE Transactions on Nuclear Science. **NS-26, No. 1** 54 (1979).
[14] A. Etkin and M.